SECOND EUROPEAN CONFERENCE ON EARTHQUAKE ENGINEERING
AND SEISMOLOGY, ISTANBUL AUG. 25-29, 2014

NUMERICAL INVESTIGATION ON THE SEISMIC RESPONSE OF HISTORICAL MASONRY STRUCTURES: LINEAR AND NON-LINEAR MODELLING OF SHAKING TABLE TESTS ON A BUILDING OF URM BEFORE STRENGTHENING

Anna KARATZETZOU[1], Konstantinos ILIOU[2], Dimitris PITILAKIS[3], Sergio LAGOMARSINO[4], Serena CATARI[5], Elisavet VITZILEOU[6], Chrissy-Elpida ADAMIS[7]

ABSTRACT

This study regards the numerical and experimental investigation of a two-storey building with timber floors made of three-leaf stone masonry without laces. Within the framework of this study, we simulated the examined building model with plane finite elements and equivalent frames (common frames as well as macro-elements) and compared the various simulation results with ones that stem from the shaking – table experiments for the same building. The studied building was tested in a 2:1 scale prototype, at the Laboratory of Earthquake Engineering of the National Technical University of Athens. A juxtaposition of the numerical results to the experimental ones reveals several benefits of the combined use of non-linear static analyses and linear and non-linear dynamic analyses.

INTRODUCTION

For the simulation of historical masonry, special theoretical concepts and software have been developed. The software packages have been calibrated and corroborated through numerous applications on data from experiments on simple structures. The assumptions involved are re-examined and so the optimization cycle starts over again.

In this study we examine the simulation assumptions for a two-storey building of three-leaf masonry with wooden floors. The specimen was tested in both its versions: (i) as-built and (ii) strengthened, but herein only the as-built version is examined. The building's overall configuration is simple and quite regular. It is therefore considered appropriate to use equivalent-frame models and specifically the macro-element modelling strategy. For these reasons, the special masonry-oriented software TREMURI (Lagomarsino et al., 2009) is considered as very suitable. Simulations are also conducted with SAP Advanced (Computers and Structures Inc., 2010), general-purpose finite element method software. In the current study, the peculiarities and challenges of historical stone masonry structures are highlighted. The experimental results were approximated and the assumptions made for the simulation were evaluated.

[1] PhD candidate, Aristotle University Thessaloniki, Thessaloniki, akaratze@civil.auth.gr
[2] MSc, Aristotle University Thessaloniki, Thessaloniki, hliou@civil.auth.gr
[3] Assistant Professor, Aristotle University Thessaloniki, Thessaloniki, dpitilak@civil.auth.gr
[4] Professor, University of Genova, Genova, sergio.lagomarsino@unige.it
[5] Assistant Professor, University of Genova, Genova, serena.cattari@unige.it
[6] Professor, National Technical University Athens, Athens, elvintz@central.ntua.gr
[7] PhD, National Technical University Athens, Athens, elpida_adami@yahoo.com

SHAKING TABLE TESTS

This two-storey building specimen has a regular geometry, with two long walls along the N-S axis and two short walls along the E-W axis, as seen on plan view, in Fig.1a. The openings are identical for the two storeys, besides a door in the East panel (Fig.1b). The material properties and geometrical characteristics adopted herein represent a frequent structure-type in stone masonry monuments, notably a three-leaf masonry with simply mounted timber floors. The structure features single-plank floors, whose joists are merely nailed to the collector beams. The middle leaf, that unites the masonry cross-section, is made of uncondensed rubble stone mortar, so as to replicate typical weaknesses of such walls.

Before the installation of a measurement array for accelerations and displacements, the specimen was additionally loaded with heavy metallic bodies at the two floors as described in Adami et al., (2012). First floor: 4.5t (9x0.5t evenly distributed), second floor: 3.0t (3x1.0t as a strip along the middle). The specimen was subjected (at the base) to sine and seismic signals (Table.1). As far as the seismic input is concerned, the Kalamata earthquake record (13/9/1986, M_s=6.2) was chosen. The acceleration time histories of Kalamata earthquake in N-S (North- South) and E-W (East- West) directions are presented in Fig.2.

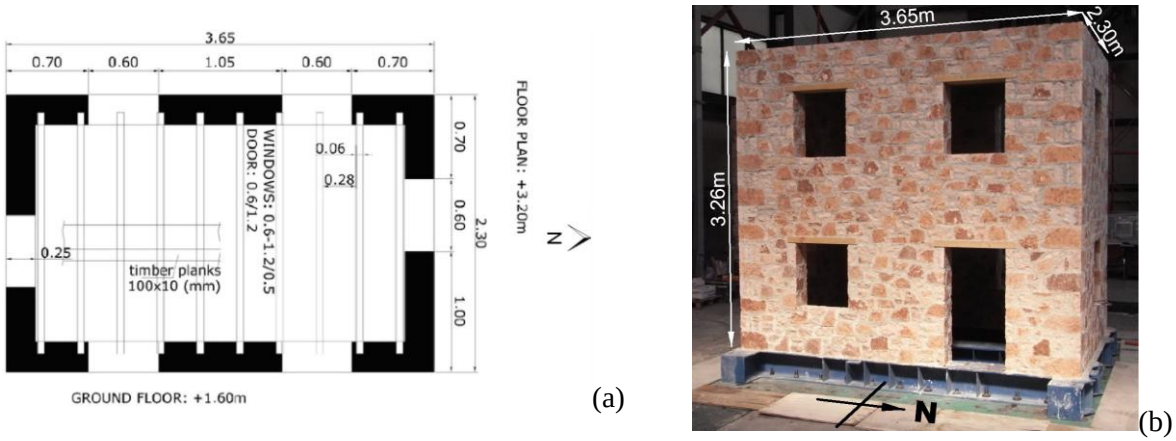

Figure 1. (a) Plan view with geometrical data and (b) general configuration and structural detail of the BM1-BS specimen; a) East face view with external dimensions (Mouzakis et al., 2012)

Table 1. Test protocol, applied for: (i) identification of initial dynamic properties under sine sweep (1BS-2BS) and (ii) inelastic response under seismic acceleration (ascending between 3BS-8BS) (Mouzakis et al., 2012, Adami et al., 2012).

No. of test	Excitation	Direction of excitation	Scale of original record	Base acceleration [g]	
				N-S	E-W
1BS	Sine sweep	N-S	–	0.02	–
2BS	Sine sweep	E-W	–	–	0.02
3BS	Kalamata	N-S & E-W	15%	0.04	0.037
4BS	Kalamata	N-S & E-W	30%	0.10	0.09
5BS	Kalamata	N-S & E-W	45%	0.14	0.13
6BS	Kalamata	N-S & E-W	60%	0.18	0.16
7BS	Kalamata	N-S & E-W	75%	0.22	0.21
8BS	Kalamata	N-S & E-W	90%	0.29	0.24

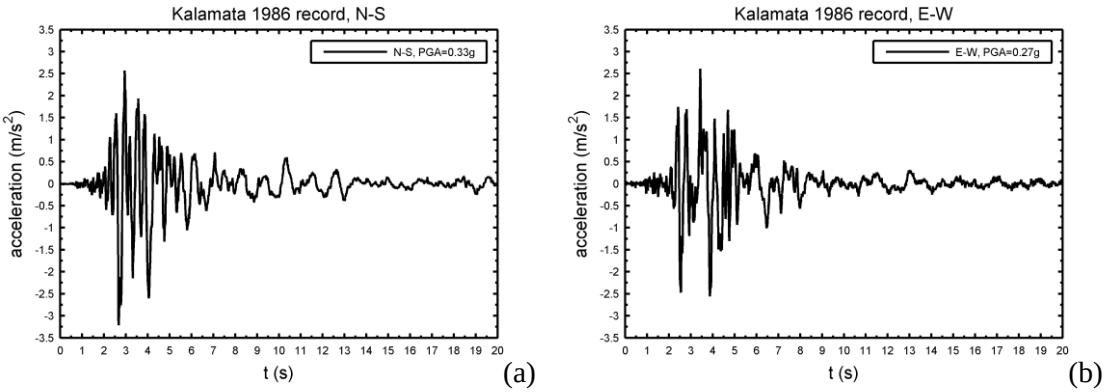

Figure 2. Base acceleration of Kalamata record (scaled), along the two axes (Karapitta et al., 2012).

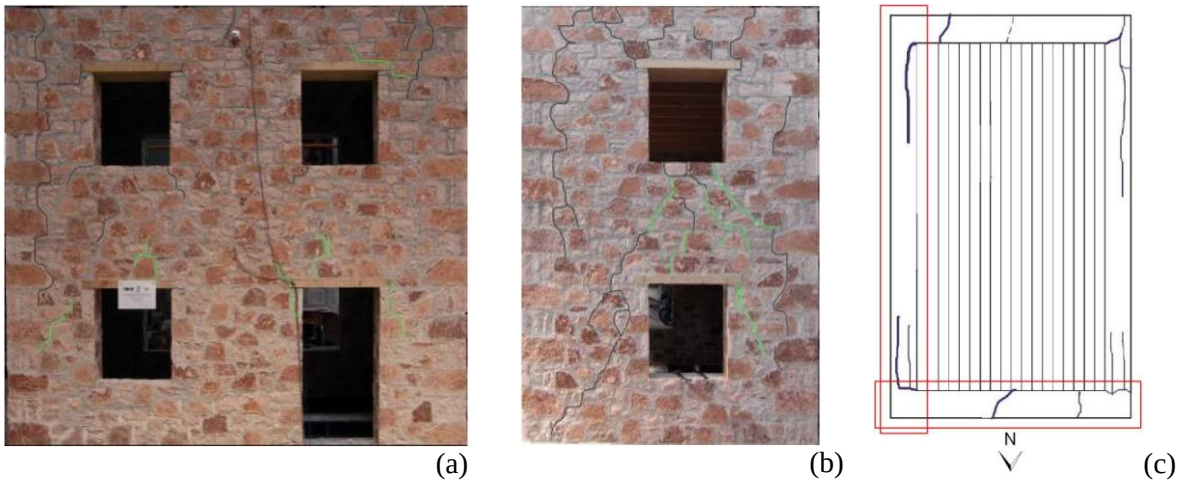

Figure 3. Crack patterns after test 8BS a) East panel and b) North panel (Adami et al., 2012) c) overall illustration of cracks at the top level plan, where one can see the corner rupture, the spandrel failure (N and S walls) and also the separation of the cross-section leafs (Mouzakis et al., 2012).

The sine-sweep tests produced along the E-W axis a dominant frequency of 4.35 Hz (i.e. T=0.230s), with a 7.01% damping ratio. Along the N-S axis, these values were f=6.10 Hz (T=0.164s) and 4.62% respectively. It is obvious that both dominant eigenvalue and damping ratio have quite different values in the two directions. According to the experimental records, this was attributed to the poor diaphragm action of the floors, which allowed an observable, local out-of-plane bending, especially along the E-W axis.

The test documentation contains observations about the overall seismic behaviour (Mouzakis et al., 2012) of building. The crack patterns are significantly different for the two wall pairs (N and S, E and W), that are grouped together, by span and orientation. Due to the insufficient diaphragm action of the floors, vertical cracks were recorded close to the edges, caused by out-of-plane bending (Karapitta et al., 2012). In addition, pronounced detachment of the masonry leafs is apparent at all the masonry elements (consider Fig.3c). This detachment started at PGA values between 0.12 g and 0.16 g, namely, between tests 4BS and 6BS.

The East and West walls are characterized by out-of-plane flexural behaviour and there are some shear cracks at the openings' corners (Fig.3a). Nevertheless, the main cracks are the vertical ones and tend to separate the East and West walls from the North and South ones (Fig.3c).

In relevant literature (Mouzakis et al., 2012), the North and South walls are described too (see Fig.3b). These walls were more prone to shear, due to their smaller aspect ratio. Likewise, vertical cracks due to out-of-plane behaviour along the E-W axis were also observed at mid-length of the North and South walls, close to their top. The width of these vertical cracks decreases from top to bottom. The measured width values after test 8BS were, approximately 8mm at the top floor level, 6.5-

7mm at the level of the top storey window lintel or 5mm at the level of the top storey window base. In other words, the building is virtually split in two loosely coupled halves, the East and the West.

To conclude, the observed damage patterns were predominantly non-standard. One main aspect was the tensile failure of spandrels in the short walls, together with shear damage. There was also rupture at corners (vertical cracks in Fig.3) and separation of the cross-section leafs of the long walls (Fig.3c), symptoms which are correlated to their pronounced out-of-plane deflection.

NUMERICAL ANALYSES

Several numerical models were developed, with different approaches for simulating the masonry panels. These numerical models could be divided into three groups: (i) linearly elastic models with shell elements, (ii) linearly elastic models with equivalent frame elements and (iii) models with macro-elements. The first two were implemented in SAP Advanced and the third one in TREMURI. In literature there is also an earlier study that concerns the studied building, where a non-linear model made of shell elements was used (Karapitta et al., 2012). Timber elements were simulated as elastic frames in all the above models, since they had not been apparently damaged during the experiments.

The initial calibration of groups (i) and (ii) was carried out within the elastic range and more specifically with modal analyses and static analyses for gravity loads. These analyses led to an early evaluation of the initial assumptions regarding geometry, connectivity, mass distribution and the elastic properties of masonry (considered herein as an equivalent composite material). The assumed elastic properties of masonry walls are as follows: density: ρ_W =1.90 t/m^3, modulus of elasticity: E_W =0.230 GPa and shear modulus G_W =0.092 GPa, (roughly estimated as 0.40E_W, Stylianidis and Ignatakis, 2011). All timber elements were made of coniferous wood, classified as "Softwood C22" (Adami et al., 2012), so the respective data were adopted from literature (Winter, 2008). Further linear dynamic analyses were based on one of the shell models from group (i), the LSW model (Fig.4.a). The connectivity assumptions were identical to those in the non-linear reference model NLR (Karapitta et al., 2012). As far as the elastic domain is concerned, LSW model is considered as the closest one to NLR. The four-node shell elements in the LSW model were refined using a rectangular mesh with a maximum length of 0.10m (Fig.4a). Rigid frames of zero mass are utilized to connect collector beams' frames to the middle surface of shells as well as to fit the floor's frame mesh to the wall's shell mesh. Meanwhile, a macro-element model, named herein as NLM model, with the same elastic features as LSW model, was used for static pushover analyses (Fig.4b) and for non-linear dynamic analyses. Strength values for the properties of NLM stem from Karapitta et al., 2012. Additional modal analyses on the frame models were used to verify the automatic meshing in TREMURI. The equivalent frames were re-implemented in SAP Advanced, for a better understanding of the involved assumptions, such as the choice of effective pier height H_p (Lagomarsino et al., 2013).

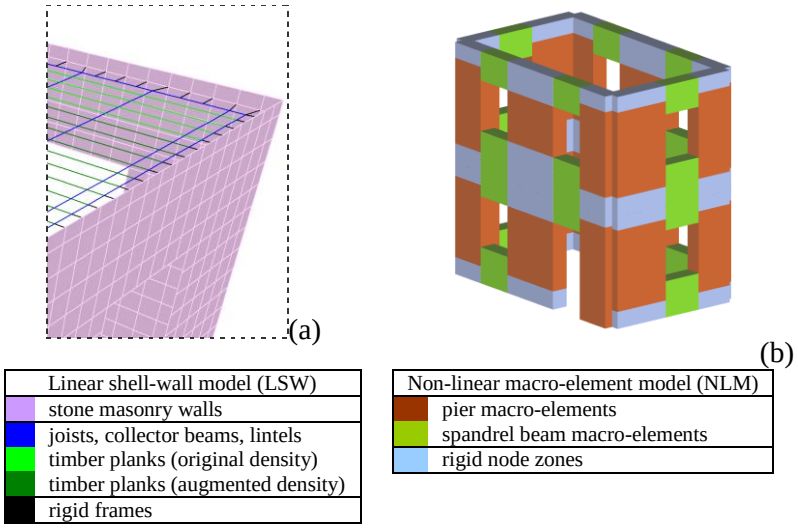

Figure 4. a) Detail from a 3D view of LSW model (top of NW corner), where the listed section types are visible; b) extruded 3D view of NLM model, where the 2D macro-elements are denoted.

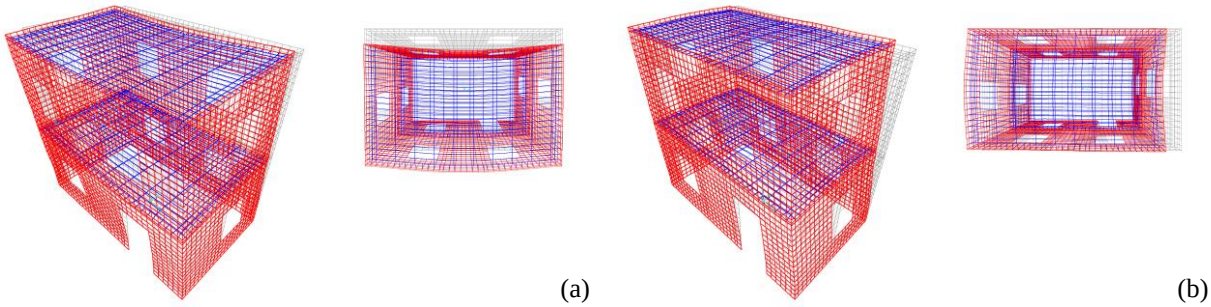

Figure 5. Dominant numerical eigenmodes in LSW model; a) first, translational along E-W axis, b) second, translational along N-S axis.

Modal identification and transfer functions

The two dominant eigenmodes are translational, along the two horizontal axes. These two modes contributed a modal participating mass ratio higher than 73% in all models. This has to do with the concentration of significant additional masses at the floor levels of the specimen, which brings the dynamic identity of this continuous-mass system closer to a discrete-mass one. Table.2 shows the two dominant translational eigenvalues of models LSW and NLM, which can be compared to the experimental ones and to those from NLR model. The eigenmodes in Fig.5 agree to the ones from the NLR model (Karapitta et al., 2012). From Table.2 it seems that the NLM model from TREMURI gives a better agreement with the experimental values.

The translational eigenmodes are the first and second one in all models except the NLM equivalent frame model. The early appearance of a torsional eigenmode can be attributed to the fact that TREMURI, with its discretization into four 2D walls, fails to consider the torsional stiffness of masonry elements. This results in a lower overall torsional stiffness, hence higher periods and participation ratios for torsional modes. One can conclude that dynamic analyses of satisfactory accuracy could be executed with these modes alone. After modal analyses, we carried out linear time-history analyses, in order to estimate the transfer functions between the base and specific measurement points at the top level of the structure. This is in fact a further modal investigation, point-by point.

Table 2. Period eigenvalues for the dominant eigenmode along each direction.

Direction	Experimental (s)	NLR (s)	LSW (s)	NLM (s)
E-W	0.230	0.205	0.203	0.225
N-S	0.164	0.152	0.155	0.157

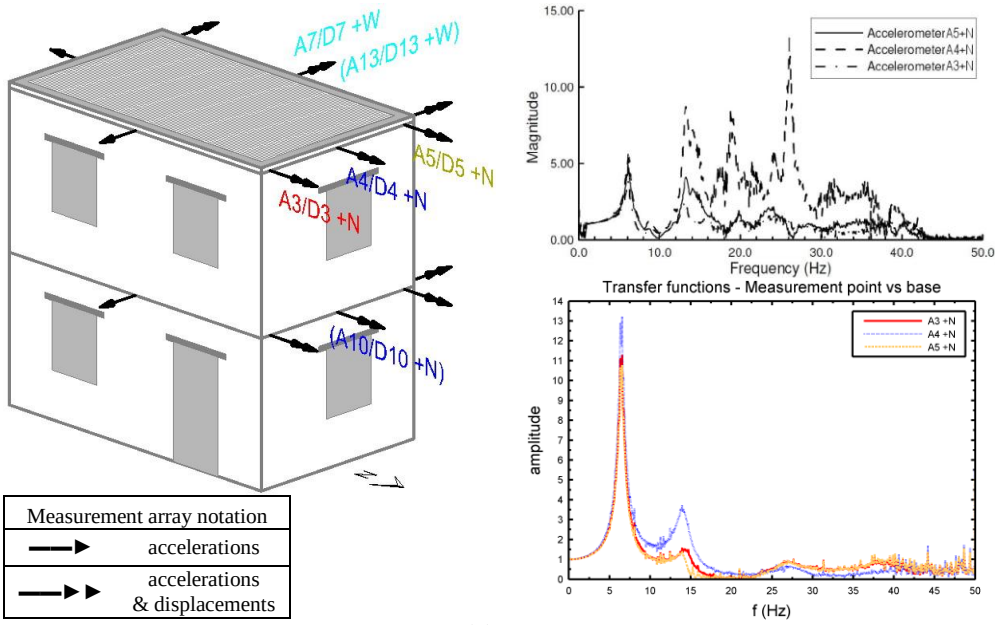

(a) (b)

Figure 6. a) Definition of recorded DOFs: colour coding and kinematic variables; b) transfer functions along the N-S axis, at the top of the North panel, top: experimental-black (under test 1BS, adapted from Mouzakis et al., 2012), bottom: LSW model-coloured.

The experimental transfer functions are acquired for the two low-amplitude, sine-sweep tests (1BS, 2BS, Table.1) in order to consider the undamaged building. The original stiffness was assumed and each of the two input signals was applied separately, to obtain independent horizontal response records. Instrumentation at record points and results are presented in Fig.6.

The experimental transfer functions (Fig.6b, top) are quite unconventional, especially that of midpoint A4+N. It contains many high-frequency peaks, whose amplitude is not strictly decreasing with frequency. It is obviously much different from that of A3+N and A5+N, since the top floor's behaviour is affected by local phenomena. The LSW model (Fig.6b, bottom) can detect the first two peaks of all response ratios, overstressing the dominant peak and slightly underestimating the secondary. But higher vibration modes of local nature remain mostly undetected; the model specifically fails to represent the special shape of high-frequency peaks in the A4+N ratio. On the other hand, the two dominant peaks of A4+N appear higher than those of A3+N and A5+N, which is more distinguishable for the second peak. So, local effects are still expressed somehow.

These results demonstrate the difficulties that can arise in elastic modelling, due to several response aspects, sometimes of a non-linear nature. Some effects are difficult to quantify and simulate, such as local out-of plane vibration of walls. Effects like these could be described by non-linear approaches of the discrete class, such as macro-block modelling or discrete interface modelling (Calderini et al., 2010).

Linear time-history analyses – response history at measurement points

The inelastic response during the final test 8BS, was approximated using equivalent linear time-history analyses, with a modal combination of all modal response histories. Input motions were introduced with equally reduced amplitudes. The reduction factor "q" was derived from the global ductility index, which was found $\mu \simeq 2.1$ from static pushover analyses that will be described in the following paragraphs. Since the dominant system periods came out very low, the "equal energy" formula was adopted, which yielded q=1.7. The viscous damping ratio was also considered as spatially constant, so we applied the experimental average in both directions, ξ=5.5%. Another basic assumption about the damaged state, was that of a reduced masonry stiffness (half the original, i.e. E_{cr}=0.115 GPa), applied uniformly to all shells, rather than selectively to assumed "cracked zones". The presented approach combines benefits from both analysis types: non-linear static and linear dynamic. The contribution of higher modes is accounted, the viscous damping part is directly

introduced, while the hysteretic part results from the pushover application. The utilized approach is based on the assumption that, during test 8BS, the specimen is near its ultimate limit state, namely $U_{8BS} \simeq U_{ULS}$. Nevertheless, the NLM model, cannot describe adequately the out-of-plane behaviour and the special features of the observed failure mechanism. In addition, the aforementioned assumptions about a spatially uniform distribution of variables, could potentially oversimplify the problem. However, during the calibration process, it was shown that these rough choices could give fairly realistic results in terms of acceleration amplitudes, hence seismic loads.

LSW approximated the experimental values quite well in terms of average maximum acceleration values of time histories at the top floor level, along both axes (Fig.7). Along N-S axis, the numerical value was 0.34g (vs 0.35g) and along E-W axis, the value was 0.44g (vs 0.48g). This -8% divergence along the E-W axis could be associated to the special nature of the overall damage mechanism. As observed, the building split at the North and South wall spandrels and behaved like two partially coupled subassemblies, in that direction. Those effects cannot be described by LSW model. In both directions, the numerical acceleration distribution is the expected one: the value at mid-length appears larger than those at the corners (Fig.7). As it was shown in a further juxtaposition of the full LSW histories, this is valid throughout the whole 10 s. Along the N-S axis; this distribution is actually close to the experimental one. Moreover, it seems that this model also takes into account the difference between the accelerations in A3+N and A5+N (refer also to Fig.6a). However, parallel to the E-W axis, the aforementioned distribution fails to simulate the experimental one, in which values grow linearly from left to right, i.e. from South to North (Fig.7).

In summary, the actual post-elastic motion is not purely translational, but more like translational-rotational around a pole, located to the S-SW of the building. This motion is obviously caused by a disruption of the initial, almost symmetrical stiffness distribution, which had caused the dominant modes to consist of translational motion alone. Indeed, a precursory application of the lateral force procedure (Fajfar and Kreslin, 2012) on a simplified version of LSW, yielded negligible static eccentricities between the mass center and the factitious elastic axis: e_{oX}=-0.016m, e_{oY}=0.049m. A linear model cannot be expected to adapt to such stiffness redistributions. It should be also mentioned that the frequencies in time- histories from the LSW model (under 8BS signal) agree with the ones of the NLR model (under 6BS) (Karapitta et al., 2012), hence the predicted periods of the cracked system are close. This indicates that most of the stiffness reduction took place during test 6BS.

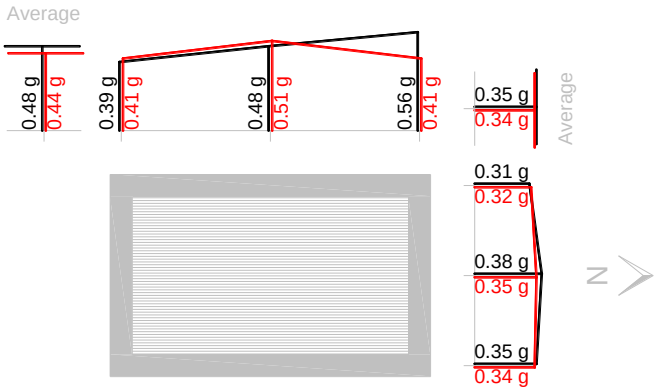

Figure 7. Acceleration amplitude distribution at the top level array (defined in Fig.7.a), under the 8BS signal; LSW model-coloured VS experimental-black.

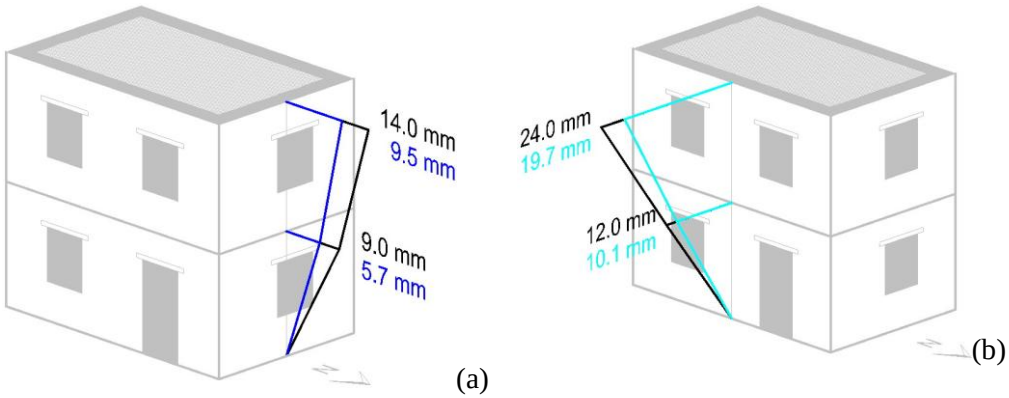

Figure 8. Displacement amplitude at mid-length; LSW-coloured VS experimental-black; a) array along N-S axis b) array along E-W axis.

Numerical displacement amplitudes at mid-length (Fig.8) deviate from the experimental ones from -16% (along E-W axis, first floor) to -37% (along N-S axis, first floor). This shortcoming is probably related to the linear nature of the model. It indicates that, even if this method proved quite effective in predicting the acceleration amplitudes, it has its limitations. Examining the relation between the two interstorey drifts, one can see that the ratio is satisfactory (Table.3). Along the N-S axis, values exhibit some divergence, but along the E-W axis they are very close to the experimental ones. In all experimental time histories, the neutral axis receives a notable permanent offset after the first 2.5s, due to the severe post-elastic deformations. Naturally, this was not the case with the LSW model, since the damage was described indirectly in it. Again, while the timing of numerical records along the N-S axis was satisfactory, the E-W records deviated a lot from the actual ones, at both levels. Just like with the acceleration values, the divergence along the E-W axis is attributed to the special features of the inelastic behaviour, which a simplified linear approach cannot simulate. It is an unconventional failure mechanism with out-of-plane motion, involving case-specific non-linear effects.

Static pushover analyses

Four pushover analyses were conducted on NLM model, for an overall examination of the post-elastic behaviour and for a rough estimation of the ductility indexes used in the linear time-history analyses. In this context, we assumed the OPCM bi-linear constitutive law (Lagomarsino et al., 2009), a first-mode load pattern and no eccentricities. The first two analyses were along the N-S axis, back and forth (i.e. ±N) and the second two along the E-W (likewise, ±W).

The strength values were adopted as in NLR model (Karapitta et al., 2012) and safety factors were set to "1". Peak compressive strength: f_{WC} =-1.50 MPa, peak shear strength: f_{WV} =0.10 MPa, residual shear strength: $f_{WV,\ lim}$ =0.05 MPa. For bending/rocking failure modes, the effect of tensile strength is ignored in "TREMURI" (Penna et al., 2013). Deformation values were defined in the macro-element scale, according to the EC8 provisions. Drift limits for shear failure and compressive-bending failure were 0.4% and 0.8%, respectively. The structure's ultimate limit state criterion was determined indirectly, at an 80% strength decay ratio. As seen in Fig.9, each bi-linear curve was drawn so that its elastic segment would intersect the original pushover curve at a force level equal to the 70% of the strength plateau.

Table 3. Calculation of drift ratios from drift values.

		Drift ratios $\Delta U_2/\Delta U_1$ [%]	
		N-S	E-W
Drifts [mm]	ΔU_2	5.0	12.0
	ΔU_1	9.0	12.0
Experimental		**56%**	**100%**
Drifts [mm]	ΔU_2	3.8	9.7
	ΔU_1	5.7	10.1
LSW model		**67%**	**96%**

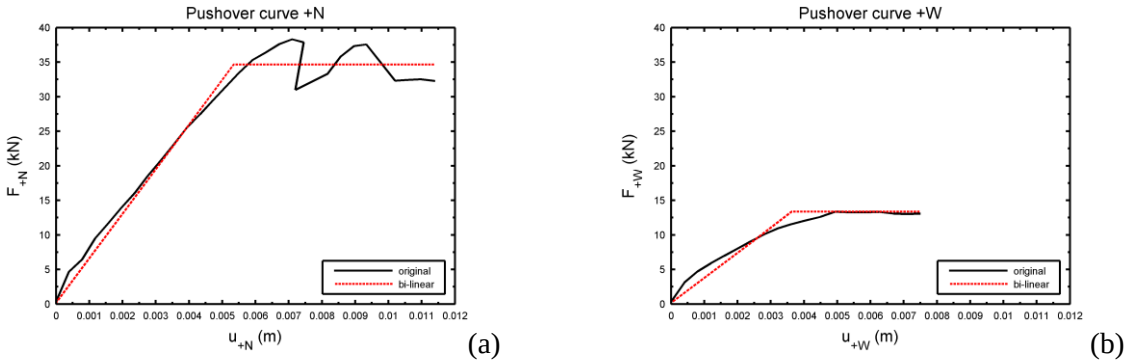

Figure 9. Static pushover curves, according to the NLM model; one case from each analysis direction is presented: a) [+N] case, b) [+W] case.

The two curves of each pair appear similar, both in terms of forces and in terms of displacements. Most curves exhibited a gradual decrease in strength. An exception was found in the post-elastic branch of the [+W] curve, which holds up until the very end and then falls suddenly, thus meeting the analysis termination criterion (Fig.9b). In Fig.9a, the [+N] curve exhibits a single point of lacking convergence, with a sudden fall and rise in strength, which is to be ignored. It was automatically marked by "TREMURI"; anyway, this anomaly is also evident from the negative step along the displacement axis. The ratios of displacements at ultimate D^u and at yield D^y, produced an almost identical average value for global ductility indexes: $\mu_{N\text{-}S} \simeq \mu_{E\text{-}W} \simeq 2.1$, in spite of the fact that the values themselves do not match perfectly, when compared for each case pair.

So, based on these pushover curves, one can estimate the achieved base shear either directly or with an indirect, mixed approach. The indirect approach uses the acquired ductility indexes to produce respective q-factors for a linear time history analysis with reduced seismic loads. As seen in Table.4, the time history analysis approximates well the base shear along N-S axis, but along E-W axis it is not as satisfactory. The strength overestimation indicates that a different q-factor could have been applied in this direction of the time-history analyses with SLW, despite the value $\mu_{E\text{-}W} \simeq 2.1$, calculated from the pushover analyses. After all, the in-plane failure mechanism assumed in the NLM model is far from the actual one in this direction, which features vertical rupture at spandrels and wall corners, followed by an out-of-plane bending of the East and West half.

Regarding the base shear values, acquired with the direct approach, they all seriously underestimate the structure's strength and probably they should be ignored. Given that the pushover analyses were executed with the commercial, design-oriented version of "TREMURI", it is possible that an internal override procedure was activated, switching the safety factors back to a set of minimum values.

In Fig.10, the plan deformation is depicted for the two pushover cases which best describe the actual, translational-rotational motion in the advanced inelastic state. The [+N] case, predicts the floors to rotate around a pole somewhere in the West side, with enhanced damage in the East wall. Likewise, the overall behaviour along E-W axis is best described by the [+W] case, which results in pronounced damage in the North wall. These deformation patterns agree with both the observed damage distribution and the measured acceleration distribution at the top level. The rotational component was not as evident in the other two cases. In Fig.11, there are the respective predictions of damage distribution for the presented cases, coloured according to the macro-element failure modes.

Table 4. Comparison of numerical extreme values for base shear to the experimental ones.

Experimental base shear **[1]**	Numerical VS experimental base shear				Experimental base shear **[1]**	Numerical VS experimental base shear		
V_N [kN]	Analysis	V_N [kN]	ΔV_N [%]		V_W [kN]	Analysis	V_W [kN]	ΔV_W [%]
61.75	Pushover case [+N]	37.93	-39%		42.83	Pushover case [+W]	13.25	-69%
	Pushover case [-N]	37.90	-39%			Pushover case [-W]	12.17	-72%
	Time history	53.96	-13%			Time history	57.73	35%

	(based on pushover)				(based on pushover)		

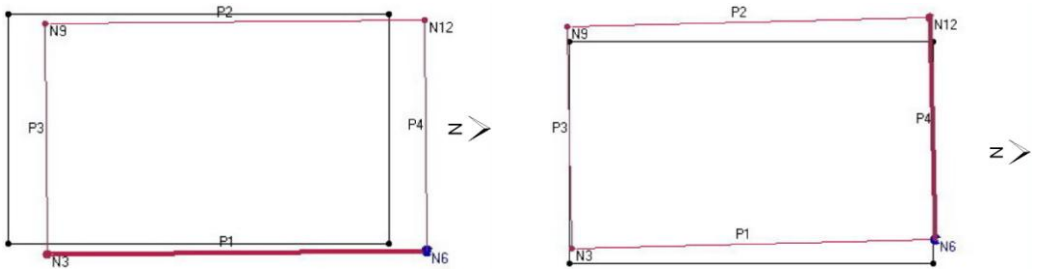

Figure 10. Top floor deformation, according to NLM model; a) [+N] case, b) [+W] case.

Figure 11. Damage distribution and failure modes (NLM model); a) [+N] case, b) [+W] case.

Damage estimation – distribution and types

We attempted a more detailed estimation of damage, with the use of LSW model. There were spotted four instants of special interest in the response history, in which the resultant base shear reached extreme values, directed at each of the four corners (NW, NE, SW, SE). This is possible, since time-history analysis allows for a monitoring of the simultaneous action of the two spatial components and a linear combination in time.

Then, failure criteria were applied, using the stress patterns at these critical instants. The EC6 failure criterion was used for shear (Stylianidis and Ignatakis, 2011), with the abovementioned strength values and also tensile stress values were checked against an assumed strength of f_{Wt} =0.15 MPa. Since the out-of-plane bending of walls occurred in an irregular manner, we ignored the bending predicted by this linear model. Namely, the stress variation in the two shell faces, related to an elastic out-of-plane bending, was neglected. The LSW results in Fig.12 regard the two most heavily damaged walls and they are compared to the experimental ones and also to those from the NLR model (Karapitta et al., 2012).

The tensile damage mapping in Fig.12a was quite different from that of the NLR. The LSW model fails to take into account the tensile cracking at the vertical edge between East and North panel. The inelastic response along the E-W axis had also manifested itself in the North panel, with vertical tension cracks over the two windows, at the spandrel beams. Indeed, the inclined tensile cracks (due to F_{11} and F_{22}) at the first floor spandrel of the North panel were predicted too. The limited vertical cracks, due to F_{11} tensile forces at the corners of East panel openings were also generally predicted in both models.

Most importantly, the downward propagation of vertical cracks at spandrel beams of the North wall was ignored in both models. Also, the NLR model failed to acknowledge the extent of the vertical crack at the common edge between the East and the North panel. At all the other corner edges, vertical cracks were ignored by both simulations. This is an important problem with the two models, since they almost end up misinterpreting the observed overall failure mechanism. The abovementioned out-of-plane phenomena, were also related to the separation of the masonry's three-leaf section, which could not be simulated by either of the employed model types.

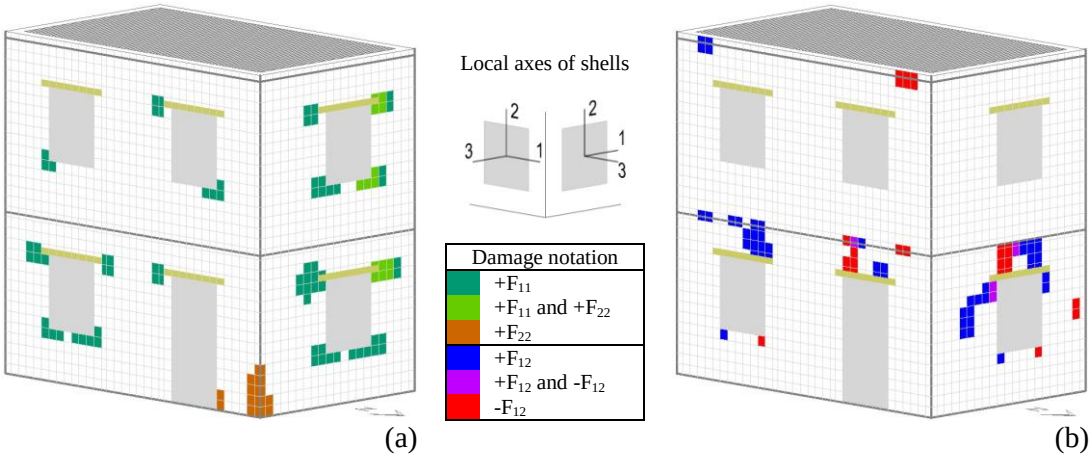

Figure 12. Expected damage distribution at the end of the 8BS load history; a) tensile damage, (b) shear damage.

The LSW model seems to predict shear damage just like the NLR model (Fig.12b), in terms of spatial distribution and of extent as well. The only exceptions were the shear cracks at the door's top-right corner (East panel) and at the North panel's bottom spandrel, which were found only in the NLR results. But such damage had not been observed, anyway.

The correlation to the actual experimental damage is satisfactory for both models. The damage incidents that were predicted by both, but did not appear, are: (i) some of the local cracks in the bottom corners of the first storey windows and (ii) the shear sliding at the floor-wall connection levels, like the horizontal cracks over the door lintel.

Both simulations are more successful in the North panel. The long, inclined crack in the North panel due to $+F_{12}$, located in the left pier of the lower storey is predicted quite accurately in the LSW simulation as well as the inclined shear-tensile cracks on the first floor spandrel beam. In the East panel, the short, inclined cracks on the first floor spandrel (left window) are predicted by both models.

Nonlinear dynamic analyses

Also a nonlinear dynamic analysis was performed on the NLM model by applying the whole accelerogram sequence in both directions (from 3BS to 8BS, as summarized in Table 1).

In particular, to this aim, the multilinear constitutive laws recently implemented in TREMURI program have been adopted (Deliverable 26, 2012). They are based on a phenomenological approach and allow to describe: 1) the nonlinear response of panels until very severe damage levels (from 1 to 5) through progressing strength decay in correspondence of assigned values of drift; 2) a quite accurate hysteretic response able to reproduce by a proper calibration of parameters the typical cycles shown by masonry panels (if flexural, shear or mixed one). Strength parameters adopted are those adopted for performing nonlinear static analyses. Regarding the drift thresholds, those assumed in nonlinear static analyses have been here adopted as corresponding to the first significant strength decay (assumed equal to 30% and 15% in case of a prevailing shear or flexural response respectively), while higher values have been assumed for the complete collapse of the elements (assumed equal to 0.007 and 0.015 in case of a prevailing shear or flexural response, respectively).

Figure 13 shows the maximum values obtained for the mean displacements at first and second levels (in N-S and E-W axis respectively) as a function of PGA of the seismic demand applied in E-W direction for each test. It is possible to observe that: 1) in agreement with some aforementioned comments, the first significant reduction in stiffness occurs in correspondence of test 6BS; 2) the values of maximum displacements are coherent with the experimental ones illustrated in Figure 10; 3) the most vulnerable direction results the transversal one (walls N and S). Indeed, the numerical simulation exhibited a more pronounced soft storey at second level than the experimental result.

Finally, Figure 14 illustrates the hysteresis loops (shear base versus mean displacement at second floor) occurred at the end of 6BS test: they confirm as the N and S walls exhibited a stronger nonlinear response. Indeed, it is important pointing out that NLM model adopted considers only the effects related to the in-plane response of walls; of course, further in-depth analyses will be addressed to analyse the role played also by the out-of-plane contribution.

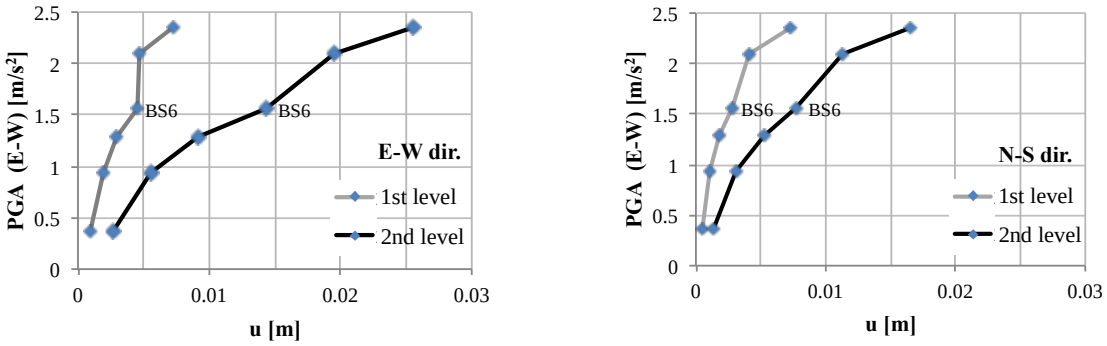

Figure 13. NLM nonlinear dynamic analyses: evolution of maximum displacements at first and second levels

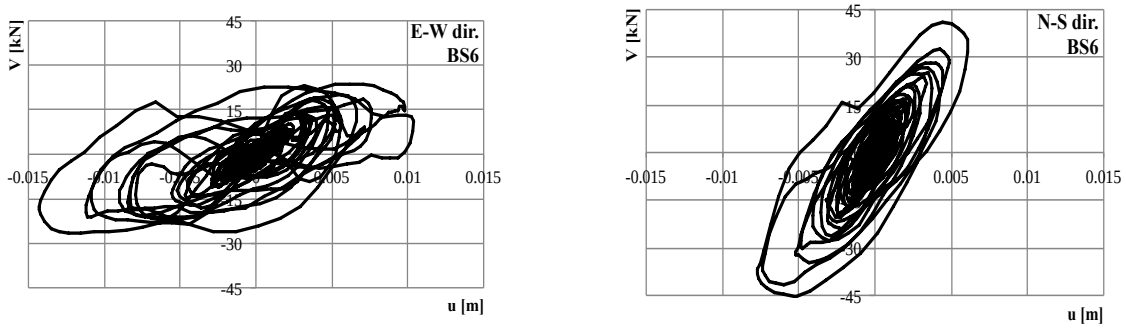

Figure 14. NLM nonlinear dynamic analyses: hysteresis loops at the end of BS6 test

CONCLUSIONS

The discussed analyses allow for the following general conclusions to be drawn: (i) the combined use of non-linear static analyses (on NLM model) and linear dynamic ones (on LSW model) exhibited certain advantages. Such advantages are: relative simplicity, a fairly satisfactory representation of both damping types and of higher-mode contribution and a realistic superposition of simultaneous response variables (e.g. the compressive and shear stress in a pier), rather than a probabilistic superposition (ii) the further potential of the macro-element approach is also revealed herein since it allows estimation of global inelastic response with a good representation of damage evolution, stiffness degradation and hysteretic damping, (iii) un-reinforced buildings of three-leaf stone masonry tend to have a unique failure mechanism, which is often hard to simulate, such as the one observed here. The out-of-plane bending with a cross-section separation and the other unique damage patterns could be adequately described only by discrete, nonlinear models. Unfortunately, their geometry is usually intricate and the calibration is very complicated and time-consuming.

ACKNOWLEDGEMENTS

This work was performed in the framework of the European project “Performance-based approach to earthquake protection of cultural heritage in European and Mediterranean countries (PERPETUATE)”, Grant agreement 244229

REFERENCES

Adami ChE, Karapitta L, Mouzakis Ch, Vintzileou E (2012) "Seismic Response of Historical Buildings Made of Three-leaf Masonry: Behaviour Enhancement with Grouting and Improvement of Box-action.", *Proceedings of the Meeting of the Hellenic Society of Earthquake Engineering "Seismic Engineering through the Scientific Perspective of Young Researchers and Engineers"*, Thessaloniki, Greece, 7 December 2012 (in Greek)

Calderini C, Cattari S, Lagomarsino S, Rossi M (2010) Review of Existing Models for Global Response and Local Mechanisms - Deliverable D7, PERPETUATE, Genova

Computers and Structures Inc. (2010) CSI Analysis Reference Manual for SAP2000®, ETABS® and SAFE®, CSI, Berkeley CA

Deliverable D26 (2012) Modelling strategies for seismic global response of building and local mechanisms. PERPETUATE (EC-FP7 Project), www.perpetuate.eu.

Fajfar P and Kreslin M (2012) "Introduction to the RC building example. Modeling and analysis of the design example.", *Proceedings of the Workshop "EC 8: Seismic Design of Buildings"*, Lisbon, Portugal, 10-11 February 2011 25-52

Karapitta L, Mouzakis Ch, Adami ChE, Vintzileou E (2012) "Non Linear Seismic Response of Three-Leaf Masonry Structures", *Proceedings of the 8th International Conference on Structural Analysis of Historical Constructions*, Wroclaw, Poland, 15-17 October

Lagomarsino S, Penna A, Galasco A, Cattari S (2009) Seismic Analysis Program for 3D Masonry Buildings - TREMURI User Guide, TREMURI Program, Genova/Pavia

Lagomarsino S, Penna A, Galasco A, Cattari S (2013) TREMURI program: an equivalent frame model for the nonlinear seismic analysis of masonry buildings, Engineering Structures, 56, pp. 1787-1799, http://dx.doi.org /10.1016/j.engstruct.2013.08.002.

Mouzakis Ch, Vintzileou E, Adami ChE, Karapitta L (2012) "Dynamic Tests on Three Leaf Stone Masonry Building Model Before and After Interventions", *Proceedings of the 8th International Conference on Structural Analysis of Historical Constructions*, Wroclaw, Poland, 15-17 October

Penna A, Lagomarsino S, Galasco A (2013) "A Nonlinear Macroelement Model for the Seismic Analysis of Masonry Buildings", *Earthquake Engineering & Structural Dynamics*, DOI: 10.1002/eqe.2335

Stylianidis K and Ignatakis Ch (2011) Structures of Load-bearing Masonry According to Eurocodes 6 & 8, Aivazi Editions, Thessaloniki (in Greek)

Winter S (2008) "EN 1995-1-1 - Design of timber structures", *Proceedings of the Workshop "Dissemination of information for training"*, Brussels, Belgium, 19 February